

A Deep Decomposition Network for Image Processing: A Case Study for Visible and Infrared Image Fusion

Yu Fu, Xiao-Jun Wu, Josef Kittler, *Life Fellow, IEEE*

Abstract—Image decomposition is a crucial subject in the field of image processing. It can extract salient features from the source image. We propose a new image decomposition method based on convolutional neural network. This method can be applied to many image processing tasks. In this paper, we apply the image decomposition network to the image fusion task. We input infrared image and visible light image and decompose them into three high-frequency feature images and a low-frequency feature image respectively. The two sets of feature images are fused using a specific fusion strategy to obtain fusion feature images. Finally, the feature images are reconstructed to obtain the fused image. Compared with the state-of-the-art fusion methods, this method has achieved better performance in both subjective and objective evaluation.

Index Terms—image fusion, image decomposition, deep learning, infrared image, visible image.

I. INTRODUCTION

IMAGE fusion is an important task in image processing. It aims to extract important features from images of multi-modality signal sources and uses certain fusion strategies to generate a fused image containing complementary information of multiple pictures. Our work is one of the common image fusion tasks, that is, to fuse visible light images and infrared images [1]. The fused images not only contain the radiation information of the occluded object, but also retain sufficient texture detail information. At present, many advanced methods are widely used in production and life, such as security monitoring, autonomous driving, target tracking, target recognition and other fields.

There are many excellent fusion methods, which can be divided into two categories: traditional methods and deep learning based methods [2]. Most of the traditional methods are based on signal processing methods to obtain high-frequency bands and low-frequency bands of the image and then merge them. With the development of deep learning, methods based on deep neural networks have also shown great potential in image fusion, because neural networks can extract features of source images and perform feature fusion.

Traditional methods can be broadly divided into two categories: one is based on multi-scale decomposition, and the other is representation learning based methods. In the multi-scale domain, the image is decomposed into multi-scale representation feature maps, and then the multi-scale feature representations are fused through a specific fusion strategy. Finally, the corresponding inverse transform is used to obtain the fused image. There are many representative multi-scale

decomposition methods, such as pyramid [3], curvelet [4], contourlet [5], discrete wavelet transform, [6], etc.

In the representation learning domain. The most methods are based on sparse representation such as sparse representation (SR) and gradient histogram (HOG) [7], joint sparse representation (JSR) [8], approximate sparse representation with multi-selection strategy [9], etc.

In the low-rank domain, Li and Wu et al. proposed a low-rank representation (LRR) based fusion method [10]. The most recent approaches, such as MDLatLRR [11] are based on image decomposition with Latent LRR. This method can extract source image features in low-rank domains.

Although the methods based on multi-scale decomposition and representation learning have achieved good performance. But these methods still have some problems. These methods are very complicated, and dictionary learning is a time-consuming operation especially for online training. If the source image is complex, these methods will not be able to extract the features well.

In order to solve this problem, in recent years, many methods based on deep learning have been proposed [2] because of the powerful feature extraction capabilities of neural networks.

In 2017, Liu et al. proposed a method based on convolutional neural network for multi-focus image fusion [12]. In ICCV2017, Prabhakar et al. proposed DeepFuse [13] to solve the problem of multi-exposure image fusion. In 2018, Li and Wu et al. proposed a new infrared and visible light image fusion method based on denseblock and autoencoder structure [14]. In the next two years, with the rapid development of deep learning, a large number of excellent methods emerged. Including IFCNN [15] proposed by Zhang et al., and fusion network based on GANs (FusionGan) [16] proposed by Ma et al., and the multi-scale fusion network framework (NestFuse) [17] proposed by Li et al. in 2020. Most of the methods based on neural networks use the powerful feature extraction function of neural networks, and then perform fusion at the feature level, and obtain the final fused image with some specific fusion strategies.

However, the method based on deep network also has some shortcomings: 1. As a feature extraction tool, neural network cannot explain the meaning of the extracted features. 2. The network is complex and takes a long time. 3. The amount and scale of infrared and visible light dataset is small, and many methods use other data sets for training. This is not necessarily suitable for extracting infrared and visible light images.

To solve these problems, we propose a novel network that

can be used to decompose images. At the same time, drawing on traditional methods and deep learning based methods, our proposed network can decompose infrared and visible light images into high-frequency feature images and low-frequency feature images to achieve better decomposition effect than traditional methods. At the same time, we design some fusion rules to fuse the high and low frequency feature images to obtain the fused feature image. Finally, these fusion feature images are reconstructed to a fused image. The method we proposed not only utilizes the powerful feature extraction capabilities of neural networks, but also realizes the decomposition of image. Compared with the state-of-the-art methods, our fusion framework has achieved better performance in both subjective and objective evaluation.

This paper is structured as follows. In Section II, we introduce some related work. In Section III, we will introduce our proposed fusion method in detail. And in Section IV, we illustrate the experimental settings, and we analyze and compare our experimental results. Finally, in the last section V, we draw a conclusion of this paper.

II. RELATED WORKS

Whether it is based on traditional image signal processing methods or deep learning based methods. They are all very reasonable and excellent methods. We will introduce some related works that inspired us in this section.

A. Wavelet Decomposition and Laplacian Filter

Wavelet transform has been successfully applied to many image processing tasks. The most common wavelet transform technique for image fusion is the Discrete Wavelet Transform (DWT) [18] [19].

DWT is a signal processing tool that can decompose signals into high-frequency information and low-frequency information. Generally speaking, low-frequency information contains the main characteristics of the signal, and high-frequency information includes the detailed information of the signal. In the field of image processing, 2-D DWT is usually used to decompose images. The wavelet decomposition of the image is given as follows:

$$\begin{aligned} M_{LL}(x, y) &= \phi(x)\phi(y) \\ M_{LH}(x, y) &= \phi(x)\psi(y) \\ M_{HL}(x, y) &= \psi(x)\phi(y) \\ M_{HH}(x, y) &= \psi(x)\psi(y) \end{aligned} \quad (1)$$

where $\phi(\cdot)$ is a low-pass filter, and $\psi(\cdot)$ is a high-pass filter. The input signal $M(x, y)$ is an image with signals in two directions. Along the x direction and the y direction, high-pass and low-pass filtering are performed respectively. As shown in Fig.1, we can get a low-frequency image which is approximate representation and three high-frequency images which are vertical detail, diagonal detail and horizontal detail respectively.

The Laplacian operator is a simple differential operator with rotation invariance. The Laplacian transform of a two-

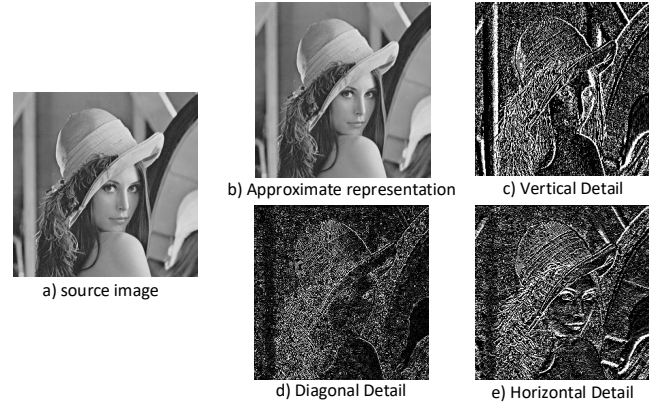


Fig. 1. Wavelet Decomposition. We perform wavelet decomposition on the image to get a low-frequency image (b) and three high-frequency images (c)(d)(e) in three directions.

dimensional image function is the isotropic second derivative, defined as:

$$\nabla^2 f(x, y) = \frac{\partial^2 f(x, y)}{\partial x^2} + \frac{\partial^2 f(x, y)}{\partial y^2} \quad (2)$$

In order to be more suitable for digital image processing, the equation is approximated as a discrete form:

$$\begin{aligned} &\nabla^2 f(x, y) \\ &\approx [f(x+1, y) + f(x-1, y) + f(x, y+1) + f(x, y-1)] - 4f(x, y) \end{aligned} \quad (3)$$

The Laplacian operator can also be expressed in the form of a convolution template, using it as a filtering kernel:

$$G_1 = \begin{bmatrix} 0 & 1 & 0 \\ 1 & -4 & 1 \\ 0 & 1 & 0 \end{bmatrix}, G_2 = \begin{bmatrix} 1 & 1 & 1 \\ 1 & -8 & 1 \\ 1 & 1 & 1 \end{bmatrix} \quad (4)$$

G_1 and G_2 are the template and the extended template of the discrete Laplacian operator, and the second differential characteristic of this template can be used to determine the position of the edge. They are often used in image edge detection and image sharpening processing, as shown in Fig.2.,

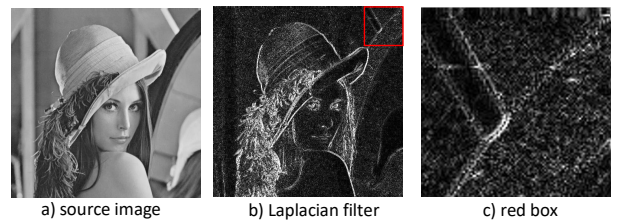


Fig. 2. Laplacian Filter. We use the Laplacian extended template for image filtering to get its high-frequency image (b), and magnify a local area of the high-frequency image (c).

We can easily observe that traditional edge filtering is usually just a high-frequency filtering. While highlighting the edges, they also highlight the noise.

B. Decomposition-based Fusion Methods

Li and Wu et al. proposed a method [11] to decompose images using low-rank representation [20].

First, LatLRR [20] can be described as the following optimization problem:

$$\begin{aligned} \min_{Z, L, E} & \|Z\|_* + \|L\|_* + \mu\|E\|_1 \\ \text{s.t.} & X = XZ + LX + E \end{aligned} \quad (5)$$

Where μ is a hyper-parameter, and $\|\cdot\|_*$ is nuclear norm, and $\|\cdot\|_1$ is l_1 norm. X is observed data matrix. Z is low-rank coefficients matrix. L is a projection matrix. E is a sparse noisy matrix.

The author use this method to decompose the image into detail image I_d and base image I_b . We can see from Fig .3 that I_d is a high-frequency image, and I_b is a low-frequency image.

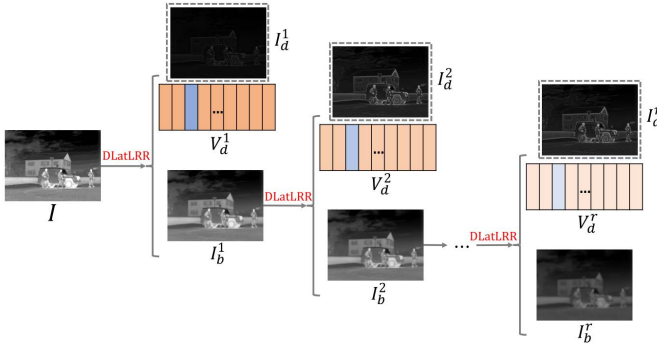


Fig. 3. The framework of MDLatLRR.

As shown in Fig .3, the low-frequency image I_b is continuously decomposed to obtain several high-frequency image I_{d1} , I_{d2} and I_{d3} .

Finally, this method decomposes the infrared image and the visible light image to obtain high-frequency images and low-frequency images. Then we perform a certain fusion to get the fused image I_f .

C. Deep Learning-based Fusion Methods

In 2017, Liu et al. proposed a neural network-based method [12]. The authors divides the picture into many small patches. Then CNN is used to predict whether each small patch is blurry or clear. The network builds a decision activation map to indicate which pixels of the original image are clear and focused. A well-trained network can accomplish multi-focus fusion tasks very well. However, due to the limitations of network design, this method is only suitable for multi-focus image fusion.

In order to enable the network to fuse visible light images and infrared images, Li and Wu et al. proposed a deep neural network (DenseFuse) [14] based on an autoencoder. First they train a sufficiently powerful encoder and decoder which can fully extract the features of the original image and reconstruct the image without losing information as much as possible. Then the infrared image and the visible light image are inputted into the encoder to obtain the coding features, and

the two sets of features are specifically fused to obtain the fusion featur. Finally, the fusion features are inputted into the decoder to obtain the fused image. These methods use the encoder to decompose the image into several latent features. Then these features are fused and reconstructed to obtain a fused image.

In the past few years, Generative Adversarial Networks(GANs) have also been applied to many fields, including image fusion. In [16] FusionGan first uses GANs to generate a fused image. The generator inputs infrared and visible light images and outputs a fused image. In order to improve the quality of the generated image, the author designed an appropriate loss function. Finally, the generator can be used to fuse any infrared image and visible light image.

In view of the superiority of these two methods, we propose a multi-layer image decomposition method based on neural network. And we propose an image fusion framework for infrared image and visible light image based on this method.

III. PROPOSED FUSION METHOD

In this section, the proposed multi-scale decomposition-based fusion network is introduced in detail. Firstly, the fusion framework is presented in section III-C. Then, the detail of training phase is described in section III-A. Next, in section III-B we give the design of the loss function of the network. Finally, we present different fusion strategy in section III-D.

A. Network Structure

In the training phase, we discard the fusion strategy and train the decomposition network.

Our training goal is to make the decomposition network better decompose the source image into several high-frequency and one low-frequency images, which are used for subsequent operations. The structure of the network is shown in Fig.4, and the detailed network settings are shown in Table I.

TABLE I
THE PARAMETERS OF THE NETWORK

Block	Layer	Channel (input)	Channel (output)	Size (kernel)	Size (input)	Size (output)	Activation
Cin	Conv(Cin-1)	1	16	3	256	256	LeakyReLU
	Conv(Cin-2)	16	32	3	256	256	LeakyReLU
	Conv(Cin-3)	32	64	3	256	256	LeakyReLU
C1	Conv(C1)	64	64	3	256	256	LeakyReLU
C2	Conv(C2)	64	64	3	256	256	LeakyReLU
C3	Conv(C3)	64	64	3	256	256	LeakyReLU
R1	Conv(R1)	64	64	1	256	256	-
R2	Conv(R2)	64	64	1	256	256	-
R3	Conv(R3)	64	64	1	256	256	-
Detail	Conv(D0)	64	32	3	256	256	LeakyReLU
	Conv(D1)	32	16	3	256	256	LeakyReLU
	Conv(D2)	16	1	3	256	256	Tanh
C-res	Conv(C-res1)	64	64	3	256	256	ReLU
	Conv(C-res2)	64	64	3	256	256	ReLU
	Conv(C-res3)	64	64	3	256	256	ReLU
Semantic	Conv(S0)	64	32	3	256	128	ReLU
	Conv(S1)	32	16	3	128	64	ReLU
	Conv(S2)	16	1	3	64	64	Tanh
Upsample	Upsample	1	1	-	64	256	-

In Fig.4 and Table I, I_{ori} is the original input image, and I_{re} is the reconstructed image. The backbone of

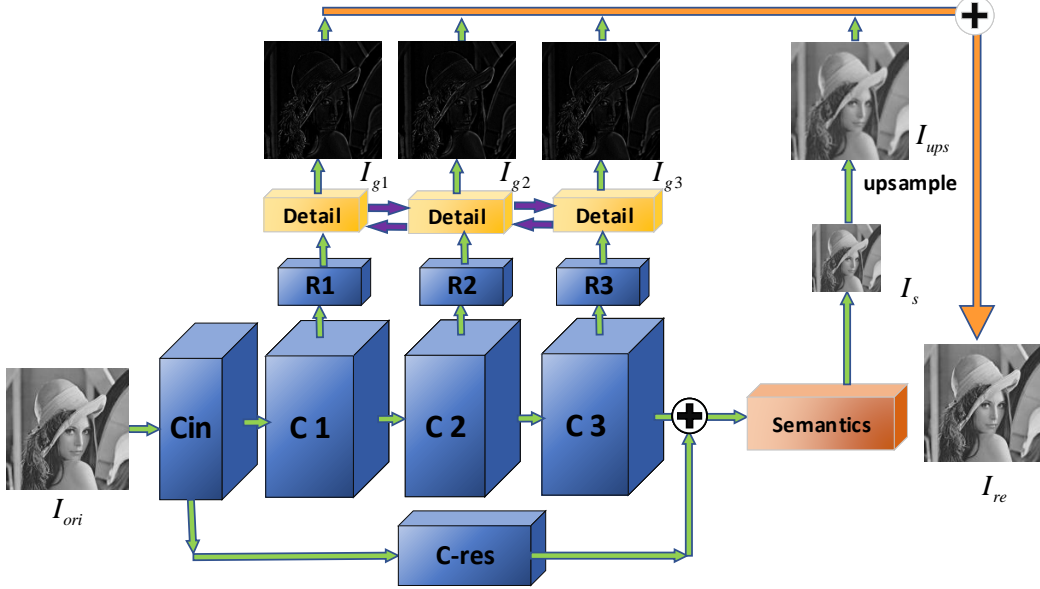


Fig. 4. The framework of training process.

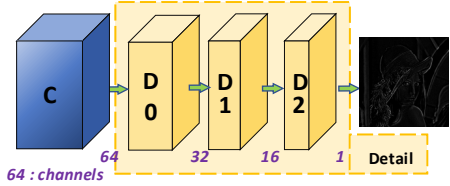


Fig. 5. We use three convolutions to reduce the channels to one and get a high-frequency image.

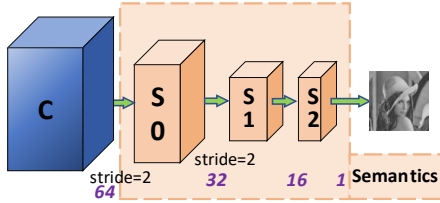


Fig. 6. We use three convolutions and downampling twice to reduce the channels to one to get a low-frequency image.

the network is four feature extraction convolutional blocks (C_{in} , $C1$, $C2$, $C3$).

Then the following is the low-frequency feature extraction part, that is, the '*semantic*' block in figure. The '*semantic*' block shown in Fig.6 include two down-sampling convolutional layers ($S0$, $S1$) with a stride of 2 and a common convolutional layer ($S3$) which can generate a low-resolution semantic image I_s . Then the I_s is up-sampled to the same size of the I_{ori} to obtain the low-frequency image I_{ups} .

We copy the features of different depths ($C1$, $C2$, $C3$) and then reshuffle their channels with convolutional layers ($R1$, $R2$, $R3$). After that, we input them into the '*detail*' branch of the shared weight to obtain three high-frequency

images I_{g1} , I_{g2} and I_{g3} . The detail branch here is shown in detail in Fig.5 and the Table I, which includes three convolutions ($D0$, $D1$, $D2$), and the number of channels is reduced to 1 to obtain a high-frequency image.

The reason for adding reshuffle layers ($R1$, $R2$, $R3$) here is that the detail block is weight-sharing, the feature maps they extract high-frequency information should follow the same channel distribution. So we add a 1×1 convolutional layer that does not share weights, and reshuffle and sort the channels of the features so that the features can adapt to the weight-shared details block.

Finally, the three high-frequency images (I_{g1} , I_{g2} , I_{g3}) and one low-frequency image (I_{ups}) are added pixel by pixel to obtain the final reconstructed image I_{re} .

Here we observe that the final reconstructed image is obtained by adding the high frequency image and the low frequency image. Therefore, the high-frequency image and the low-frequency image should be a complementary relationship in the data distribution space. When the network learns to generate images, the high-frequency image should be the residual data of the low-frequency image. So we design the residual branch (' $C - res$ ' block). We skip-connect the result of cin to the front of the *semantic* block, add it to the result of $c3$, and input it to the following layers. In this way, what $C1$, $C2$ and $C3$ get are the residual data between the source image and the semantic image, which is compulsive and natural. In order to make the skip-connected data more closely match the deep features of $C3$, we performed three convolutions in ' $C - res$ ' block to increase the semantics of the skip-connected features.

As shown in the activation function in the Table I, we consider some properties of low-frequency images and high-frequency images, we choose LeakyRelu [21] as the activation

function of the convolution of the backbone network and the high frequency part ($C_{in}, C1, C2, C3, detail$), and Relu function is used as the activation function of the convolution layers of the residual branch (' $C - res$ ') and the *semantic* block ($S0, S1, S2$). Because the output of Relu has a certain degree of sparseness, which allows our low-frequency features to filter out more useless information and retain more blurred but semantic information. Finally, in order to constrain the pixel value of the obtained image to a controllable range, we use the *Tanh* activation function after the last layer of *detail* and *semantic* block.

In general, we first perform a convolution block (*cin*) to obtain a set of feature maps containing various features. Then after three same convolution operations($c1, c2, c3$), three sets of shallow features are obtained. Then after two downsampling (*semantic*), deep feature is obtained. We believe that shallow features contain more low-level information such as texture and detailed features. We reshuffle the channels and feed these three sets of shallow features into the high-frequency branch(*detail*) to obtain three high-frequency images. What is more, we believe that deep feature has more semantic information and global information, so we convolve and upsample the deep feature to get our low-frequency images. At the same time, we use the residual branch ($C - res$) to explicitly establish the residual relationship between the high-frequency feature and the low-frequency feature. Lastly, we add these feature images pixel by pixel to get a reconstructed image.

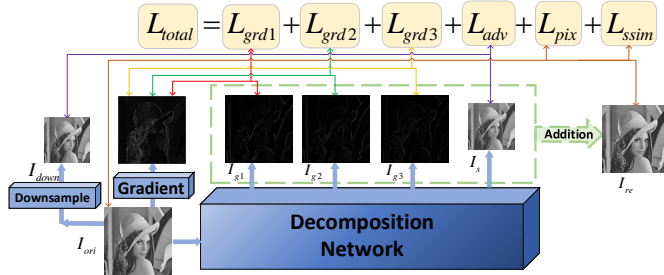


Fig. 7. The component of loss function.

B. Loss Function

In the training phase, the loss function($Loss_{total}$) of our network consists of three parts. These losses are the gradient loss(L_{detail}) of the high-frequency image, the distribution loss($L_{semantic}$) of the low-frequency image and the content reconstruction loss($L_{reconstruction}$) of the reconstructed image. The formula of the loss function is defined as follows:

$$Loss_{total} = L_{detail} + \alpha L_{semantic} + \beta L_{reconstruction} \quad (6)$$

α and β are hyper-parameters that balances the three losses.

As shown in Fig. 7, Where L_{detail} is to calculate the mean square error loss between the high-frequency feature map (I_{g1}, I_{g2}, I_{g3}) and the gradient image of the original image, and

then we accumulate these three losses. The detailed calculation formula of L_{detail} is presented as follows:

$$\begin{aligned} L_{detail} &= L_{grd-1} + L_{grd-2} + L_{grd-3} \\ L_{grd-i} &= MSE(Gradient(I_{ori}), I_{g-i}), i \in \{1, 2, 3\} \\ MSE(X, Y) &= \frac{1}{N} \sum_{n=1}^N (X_n - Y_n)^2 \end{aligned} \quad (7)$$

Where I_{ori} is the input source image and I_{g-i} is the i th high-frequency image. The $MSE(X, Y)$ is the mean square error between X and Y . The gradient image of the original image is obtained by using the Laplacian gradient operator $Gradient()$. The Laplacian operator performs a mathematical convolution operation in Equ.4.

In Equ.6, $L_{semantic}$ is a data distribution loss. We calculate a strong supervised loss of the high-frequency image, and calculate a strong supervised loss of the reconstructed image below. We hope that the low-frequency semantic block learn to extract deep semantic information, rather than giving it an answer to let it remember the answer. At the same time, we cannot give a suitable low-frequency image to the network for reference. The low-frequency information is definitely not a simply down-sampled image. But if the network does not have any loss function, it is difficult to get the low-frequency image we really want. Therefore, we use the down-sampled images as an approximate data distribution of low frequency images, so that the low-frequency results generated by our network can be in the "low frequency domain" space. The experiment in the next section proves that this loss is indeed very effective.

$$L_{semantic} = L_{adv}(I_s, I_{down}) \quad (8)$$

where I_s is the low-frequency semantic image generated by the network, I_{down} is the low-frequency blurred image obtained by downsampling the source image twice, and L_{adv} is the adversarial loss.

$$\begin{aligned} L_{adv}(I_s, I_{down}) &= L_G = \frac{1}{N} \sum_{n=1}^N (D(G(I_s^n)) - 1)^2 \\ L_D &= \frac{1}{N} \sum_{n=1}^N (D(I_{down}^n) - 1)^2 + \frac{1}{N} \sum_{n=1}^N (D(I_s^n) - 0)^2 \end{aligned} \quad (9)$$

where $n \in \mathbb{N}_N$, N represents the number of images. The loss function we use here is defined in LSGAN [22].

In Equ.6, $L_{reconstruction}$ is the image content reconstruction loss of the reconstructed image. The $L_{reconstruction}$ loss consists of two parts, one is the pixel-level reconstruction loss L_{pix} , and the other is the structural similarity loss L_{ssim} as follows:

$$L_{reconstruction} = L_{pix} + \gamma L_{ssim} \quad (10)$$

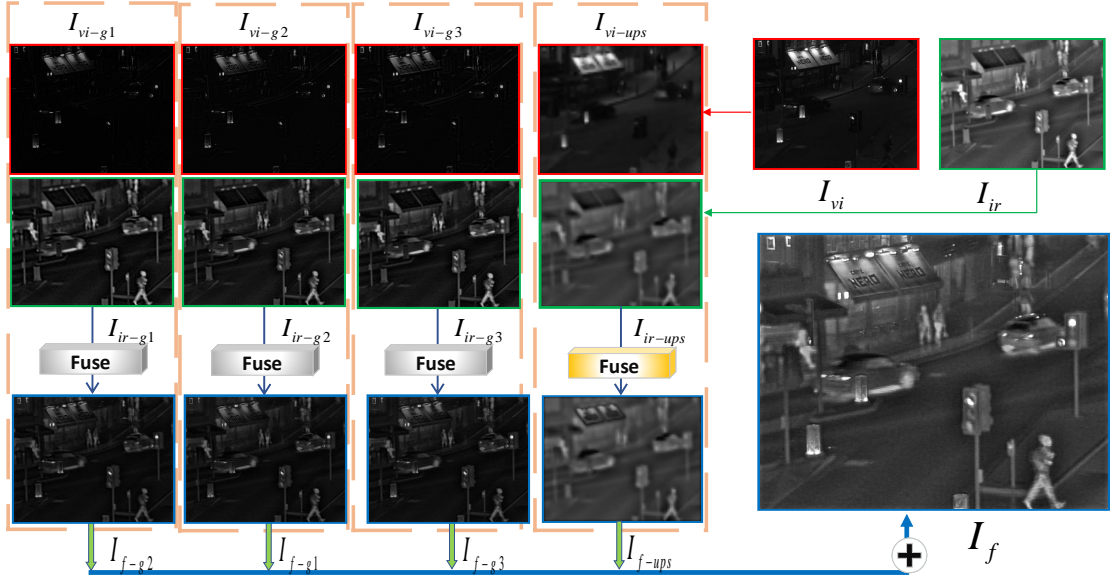


Fig. 8. Decomposition and fusion of infrared and visible images.

Where γ is a hyper-parameter that balances the two losses. L_{pixel} and L_{ssim} are calculated as follows:

$$\begin{aligned} L_{pixel} &= MSE(I_{ori}, I_{re}) \\ L_{ssim} &= 1 - SSIM(I_{ori}, I_{re}) \\ SSIM(x, y) &= \frac{(2\mu_x\mu_y + c_1)(2\sigma_{xy} + c_2)}{(\mu_x^2 + \mu_y^2 + c_1)(\sigma_x^2 + \sigma_y^2 + c_2)} \end{aligned} \quad (11)$$

As shown in the Fig. 7, the total loss function L_{total} is given as follows:

$$\begin{aligned} Loss_{total} &= L_{detail} + \alpha L_{semantic} + \beta L_{reconstruction} \\ &= L_{grd-1} + L_{grd-2} + L_{grd-3} + \lambda_1 L_{adv} + \lambda_2 L_{pix} + \lambda_3 L_{ssim} \end{aligned} \quad (12)$$

$\lambda_1, \lambda_2, \lambda_3$ are hyper-parameters and are used to balance the losses.

C. Image Fusion

In the testing phase, our fusion structure is divided into two parts: decomposition and fusion, as shown in Fig.9. The decomposition network can decompose the image into three high-frequency images and one low-frequency image. The fusion strategy ("FS" in Fig.9) can fuse the corresponding feature images and reconstruct them to obtain the final image.

In Fig.9, I_{ir} and I_{vi} represent infrared image and visible light image, respectively. The two images are fed into the decomposition network to obtain two sets of feature images. One group of feature images comes from visible light images including three visible light high-frequency images ($I_{vi-g1}, I_{vi-g2}, I_{vi-g3}$) and one visible light low-frequency image (I_{vi-ups}). And another group of feature images comes from infrared images including three infrared high-frequency images ($I_{ir-g1}, I_{ir-g2}, I_{ir-g3}$) and one infrared low frequency image (I_{ir-ups}). For the corresponding four groups of feature images, our fusion strategy contains a variety of fusion methods to obtain the final fused image I_f .

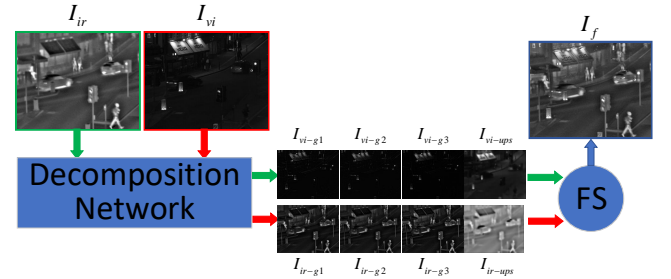


Fig. 9. The framework of proposed method. "Decomposition Network" can decompose the image and "FS" indicates fusion strategy.

In the following subsection, we will introduce the fusion strategy.

D. Fusion strategy

We design a fusion strategy to get a fused image. As shown in the Fig.8, we first use the decomposition network to decompose the visible light image I_{vi} and the infrared image I_{ir} to obtain two sets of high and low frequency feature images. The corresponding high-frequency and low-frequency feature images (such as I_{vi-g1} and I_{ir-g1}) are fused using different specific fusion strategies to obtain fused high-frequency feature images and low-frequency feature images ($I_{f-g1}, I_{f-g2}, I_{f-g3}, I_{f-ups}$). Finally, the fusion feature image is added pixel by pixel to obtain the fused image I_f , which is the same as reconstructing an image in the training phase.

We designed two fusion strategies for high-frequency image fusion, namely, pixel-wise addition (addition) and the corresponding pixel taking the maximum value (max). In addition, we also designed two fusion methods for low-frequency images, which are adding and averaging pixel by pixel (avg),

and the corresponding pixel takes the maximum value (max), as shown in Fig.10. The formulas of high frequency fusion

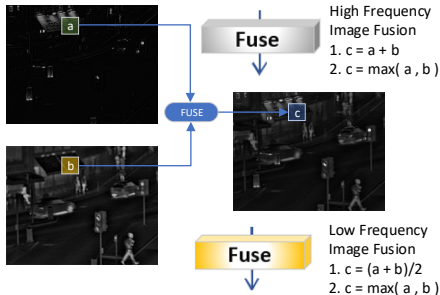


Fig. 10. High and low frequency image fusion strategy. Here a and b are any pair of points from feature images, and c is the corresponding fused pixel.

feature I_{f-g} and low frequency fusion feature I_{f-ups} are described as follows:

$$\begin{aligned} I_{f-gj}^n &= \max(I_{vi-gi}^n, I_{ir-gi}^n), & (Max) \\ \text{or } I_{f-gj}^n &= I_{vi-gi}^n + I_{ir-gi}^n & (Add) \\ I_{f-ups}^n &= \frac{(I_{vi-ups}^n, I_{ir-ups}^n)}{2}, & (Avg) \\ \text{or } I_{f-ups}^n &= \max(I_{vi-ups}^n, I_{ir-ups}^n) & (Max) \\ i &\in \{1, 2, 3\}, n \in \mathbb{N} \end{aligned} \quad (13)$$

Where i represents three high-frequency images, and \mathbb{N} represents all pixels in the image. I_{vi-gi}^n and I_{ir-gi}^n are any pixel in the corresponding three groups of high-frequency images, and I_{vi-ups}^n and I_{ir-ups}^n are any pixel in the low-frequency image. We calculate and fuse the corresponding pixels to get the pixels of the fused high frequency image I_{f-gj}^n and low frequency image I_{f-ups}^n . Finally, the three fusion features are added to obtain the final fused image I_f as follows:

$$I_f = I_{f-g1} + I_{f-g2} + I_{f-g3} + I_{f-ups} \quad (14)$$

IV. EXPERIMENTS AND ANALYSIS

A. Training and Testing Details

For the selection of hyper-parameters, we make the values of losses as close to the same order of magnitude as possible. So, in formula 12, we set $\lambda_1 = 0.1$, $\lambda_2 = 100$, $\lambda_3 = 10$ by cross validation.

Our goal is to train a powerful decomposition network that can decompose images into high-frequency and low-frequency images well. In this way, our input images in the training phase are not limited to infrared images and visible light images. We can also use MS-COCO [23] and Imagenet [24] or other images to achieve this goal. In our experiment, we use MS-COCO as the training set to train our decomposition network. We select about 80,000 images as input images. These images are converted to gray scale images which are then resized to 256×256 .

We select twelve pairs of infrared and visible light images from the TNO [25] as our test images. The reason why the

TNO dataset is not used as training data is that the TNO dataset has few pictures and is suitable for testing. At the same time, we select fifty pairs of infrared and visible light images from the RoadScene dataset [26] for testing.

We input batchsize of 64 images to the network every iteration. And, we select Adam [27] iterator and adaptive learning rate decay method [28] as the learning rate scheduler. We set the initial learning rate to $1e-3$, the attenuation factor to 0.5, the maximum patience to 5 iterations, and the minimum learning rate threshold to $1e-8$. We set the maximum number of epochs to 1000.

In the test phase, because our network is a fully convolutional network, we input infrared images and visible light images without preprocessing operations.

The experiment is conducted on the two NVIDIA TITAN Xp GPUs and 128GB of CPU memory. We decompose 1000 images with 256×256 resolution one by one and calculate the average calculation time. It takes about 2ms to decompose each image.

B. the role of the adversarial loss

As shown in Fig 11, if we do not give constraints on the low-frequency image I_s , it is difficult for the network to learn smartly to get a semantic low-frequency image we want. Without the distribution loss function, the high-frequency images learned by the network have too much semantic information, such as the distribution of colors-this is not high-frequency information. And low-frequency images loses a lot of semantic information.

In order to allow the *semantic* block to learn the real low-frequency information we want, we give it a hint that is the weak supervision loss. As in Equ. 9, we regard the down-sampled image I_{down} as an approximate solution of the low-frequency image, so that the low-frequency image I_s generated by the network follows the distribution of the low-frequency images.

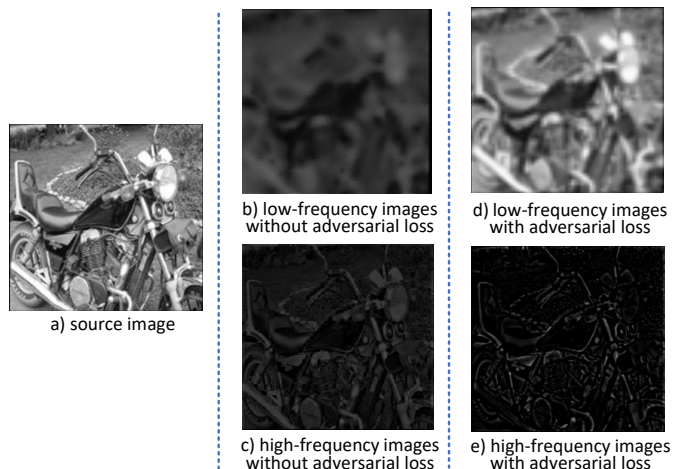


Fig. 11. The effect of adversarial loss. a) is the original image, b) and c) is the high-frequency image and low-frequency image without adversarial loss, and d) and e) is the result of using adversarial loss.

C. the details of the decomposed images

Although the loss function of our high-frequency image is calculated with gradient map which is calculated by Laplacian operator. But the result of our high-frequency image is quiet different from the Laplacian gradient high-frequency image.

As shown in Fig 12, we list the high-frequency images decomposed by the proposed decomposition network and the Laplacian operator. It can be seen that the Laplacian gradient images only extract part of the high-frequency information, and the image has a lot of noises.

The high-frequency image decomposed by our decomposition network not only retains almost all high-frequency information on the basis of the Laplacian gradient image, but also completely extracts the contour and detail information of the object. In addition, our high-frequency images have a certain degree of semantic recognition, and can clearly express the semantic features according to the outline of the objects.

D. Comparison with State of The Art Methods

We select ten classic and the state of the art fusion methods to compare the fusion effect of our proposed method, including Curvelet Transform (CVT) [29], dualtree complex wavelet transform (DTCWT) [30], Multi-resolution Singular Value Decomposition (MSVD) [31], DenseFuse [14], the GAN-based fusion network (FusionGAN) [16], a general end-to-end fusion network(IFCNN) [15], MDLatLRR [11], NestFuse [17], FusionDN [26] and U2Fusion [32]. We use the public codes

of these methods and the parameters shown in the paper to obtain fused images.

Because there is currently no clear specific evaluation indicators to measure the quality of the fused image, we will comprehensively compare it according to the subjective evaluation and the objective evaluation respectively.

1) *subjective evaluation*: In different fields, for different tasks, everyone has his/her own criteria for judging. We consider the subjective feelings of the picture, such as lightness, fidelity, noise, and clarity etc.

In Fig. 13 and Fig. 14, our method is compared with other methods. It can be clearly seen that our fused image not only perfectly retains the radiation information of the infrared image, but also fully retains the detailed texture information of the visible light image. More importantly, our image does not have a lot of noises. We marked some salient areas with red boxes. For example, in Fig. 13, the canopy of the shop has less noises. In Fig. 14, the outline of the person in the distance is clearly visible..

2) *objective evaluation*: Subjective feelings have great personal factors, and it is not enough for evaluation to rely solely on subjective evaluation. We select fifteen objective evaluation indicators from the popular objective indicators for comprehensive evaluation. They are: Edge Intensity(EI) [33], SF [34], Entropy (EN) [35], Sum of Correlation Coefficients (SCD) [36], Fast Mutual Information (FMI_w and FMI_{dct}) [37] ,Mutual Information (MI) [38], Standard Deviation of Image (SD), Definition (DF) [39], Average gradient (AG) [40]

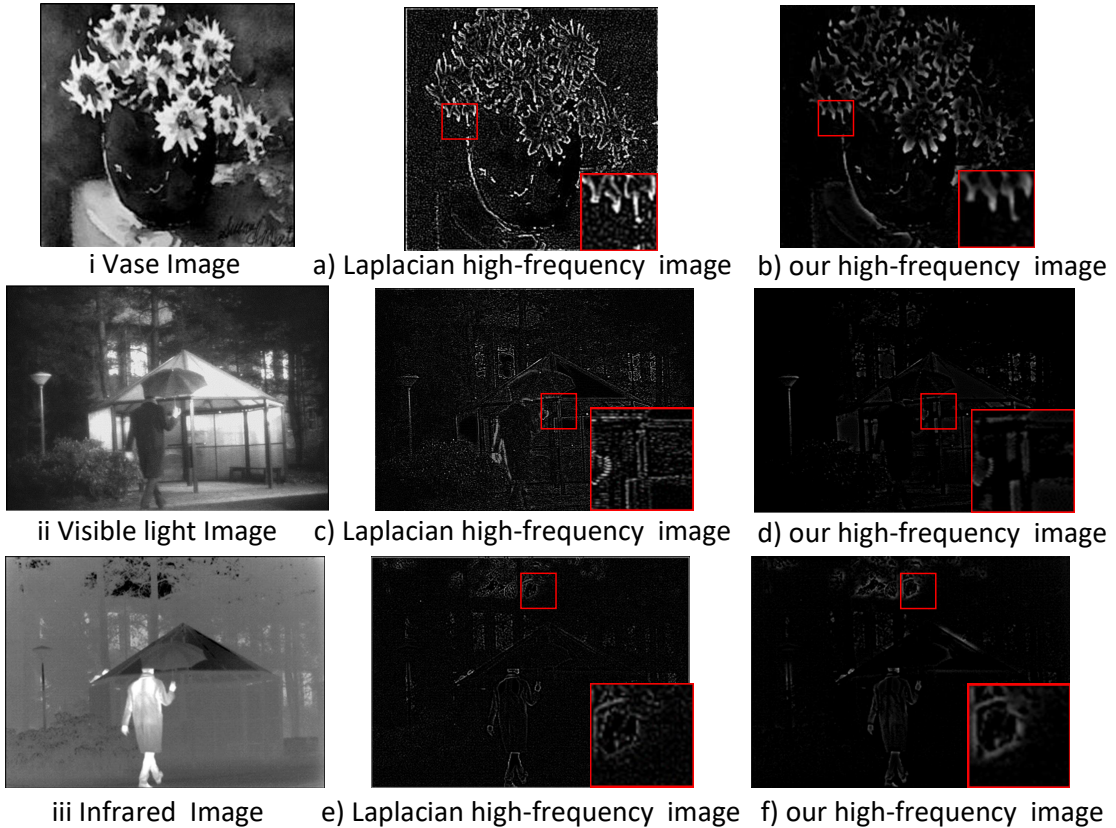


Fig. 12. High-frequency images decomposed by the proposed decomposition network and the Laplacian operator.

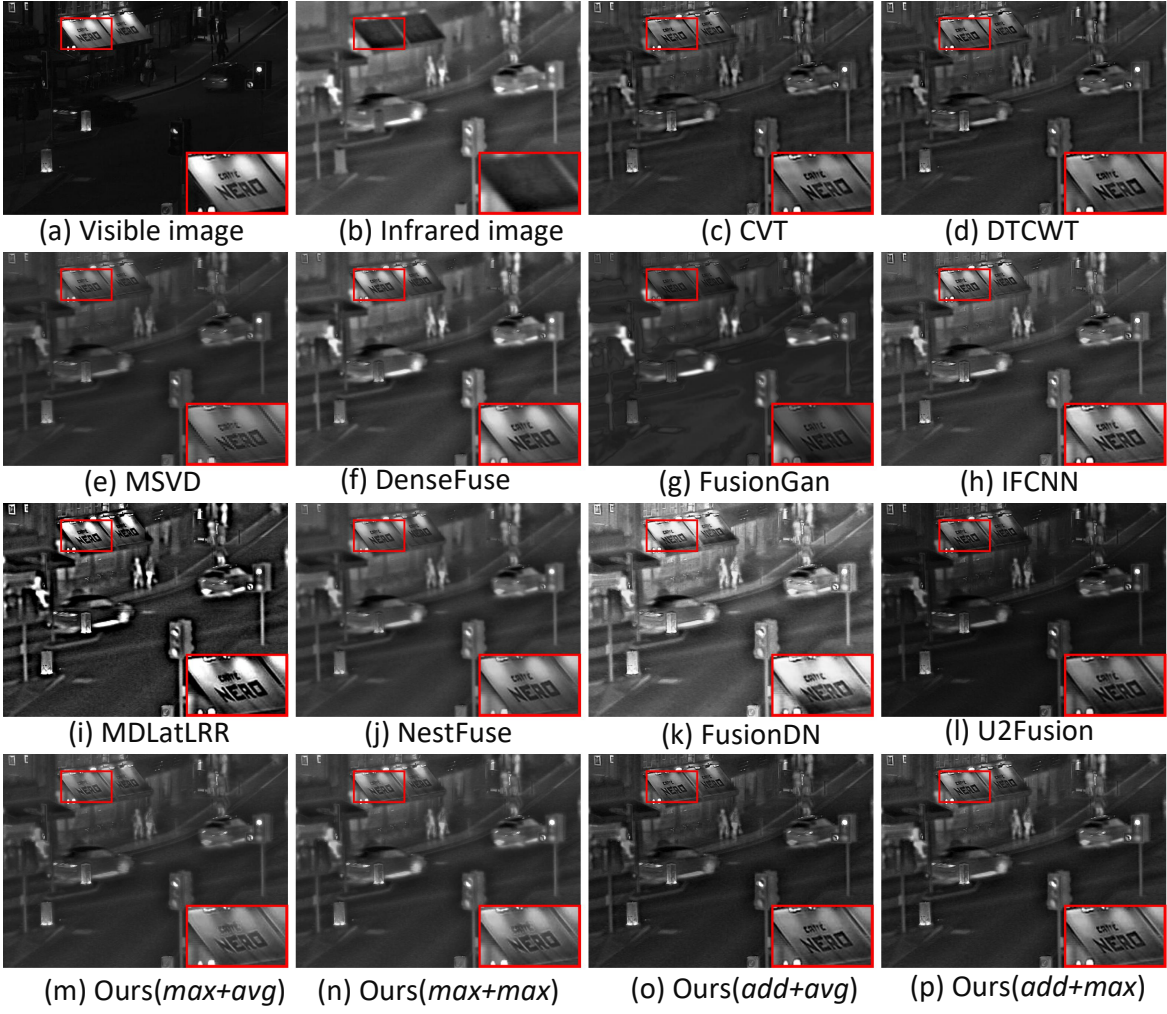


Fig. 13. Experiment on street images.

TABLE II
OBJECTIVE EVALUATION OF CLASSIC AND LATEST FUSION ALGORITHMS ON TNO DATASET

Methods	EI	SF	EN	SCD	FMI_w	FMI_dct	MI	SD	DF	AG	QG
CVT	42.9631	11.1129	6.4989	1.5812	0.4240	0.3945	12.9979	27.4613	5.4530	4.2802	0.4623
DTCWT	42.4889	11.1296	6.4791	1.5829	0.4419	0.3936	12.9583	27.3099	5.4229	4.2370	0.5024
MSVD	27.6098	8.5538	6.2807	1.5857	0.2828	0.2470	12.5613	24.0288	4.2283	2.8773	0.3375
DenseFuse	36.4838	9.3238	6.8526	1.5329	0.4389	0.3897	13.7053	38.0412	4.6176	3.6299	0.4569
FusionGan	32.5997	8.0476	6.5409	0.6876	0.4083	0.4142	13.0817	29.1495	4.2727	3.2803	0.2784
IFCNN	44.9725	11.8590	6.6454	1.6126	0.4052	0.3739	13.2909	33.0086	5.9808	4.5521	0.4864
MDLatLRR	28.0985	7.3383	6.3016	1.6043	0.4296	0.4080	12.6032	24.7217	3.5486	2.7938	0.4127
NestFuse	38.4401	9.7098	6.8856	1.5839	0.4504	0.3694	13.7713	38.3311	4.9099	3.8376	0.4895
FusionDN	61.3491	14.2256	7.4073	1.6148	0.3651	0.3159	13.6147	48.5659	7.4565	5.9832	0.3785
U2Fusion	48.4915	11.0368	6.7227	1.5946	0.3594	0.3381	13.4453	31.3794	5.8343	4.7392	0.4039
Ours	max + avg	30.1185	8.0322	6.3621	0.7133	0.1282	0.0984	12.7242	25.2654	3.9611	3.0370
	max + max	33.5991	8.4408	6.6711	0.6959	0.1299	0.0985	13.3422	38.5077	4.1961	3.3191
	add + avg	46.0222	12.0192	6.5235	0.6629	0.1278	0.0984	13.0470	27.4135	6.1148	4.6537
	add + max	48.5475	12.3100	6.8973	0.6748	0.1293	0.0984	13.7945	39.9003	6.2682	4.8526
and QG [33] respectively.											

The objective evaluation indicators here are divided into two categories. One is to evaluate the fused image, such as calculating the edge(EI), the number of mutations in the

image(SF), average gradient(AG), entropy (EN), clarity(DF) and contrast of the image(SD). The other is to evaluate the fused image with the source image. There is another category that evaluates the fused image and the source image, such as

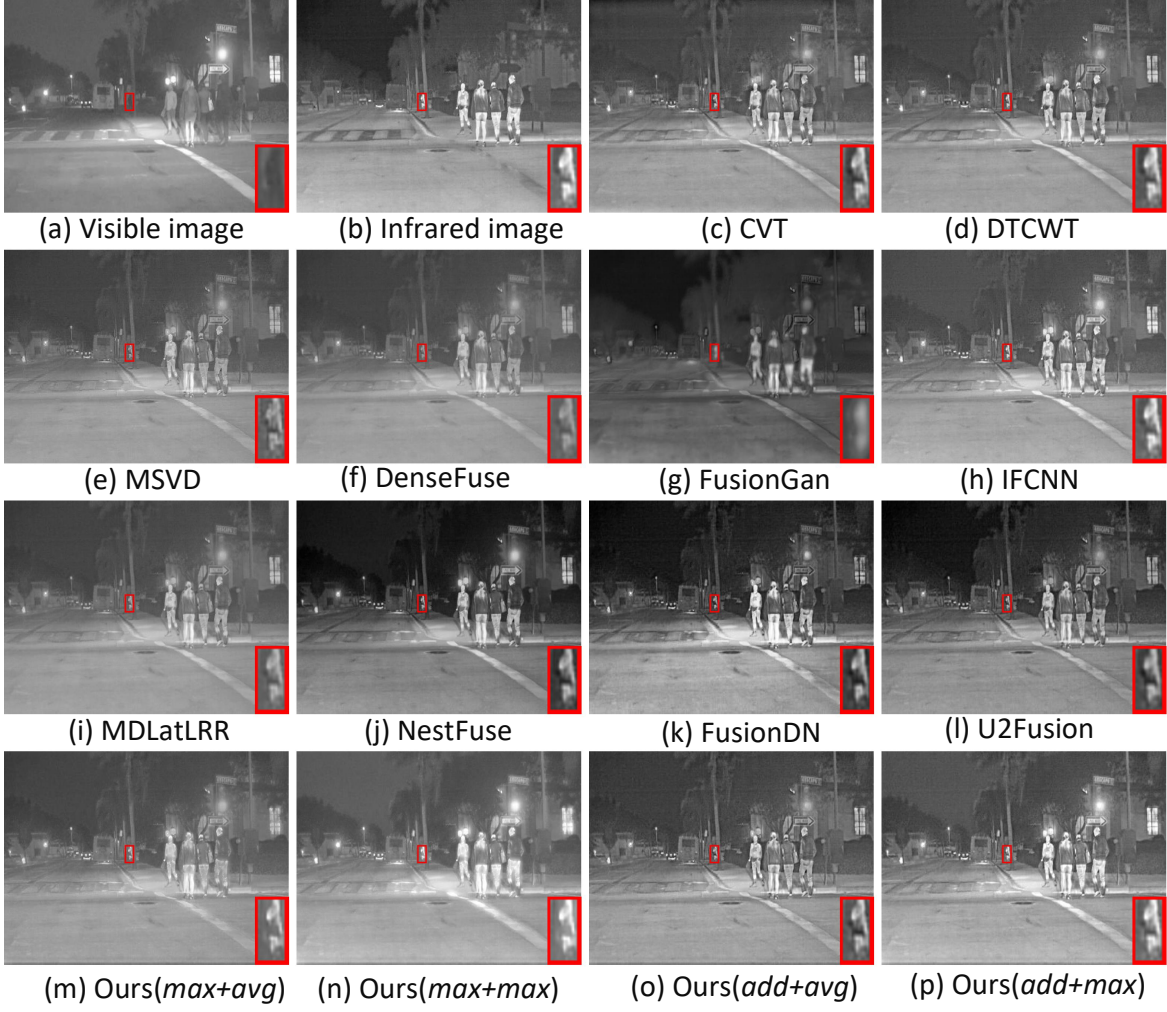


Fig. 14. Experiment on road images.

TABLE III
OBJECTIVE EVALUATION OF CLASSIC AND LATEST FUSION ALGORITHMS ON ROADSCENE DATASET

Methods	EI	SF	EN	SCD	<i>FMI_w</i>	<i>FMI_{dct}</i>	MI	SD	DF	AG	QG
CVT	59.7642	14.7379	7.0159	1.3418	0.4138	0.3631	14.0319	36.0884	6.9618	5.7442	0.4499
DTCWT	57.3431	14.7318	6.9211	1.3329	0.3458	0.2383	13.8421	34.7264	6.7810	5.5228	0.4402
MSVD	36.0475	11.3182	6.6960	1.3458	0.2659	0.2195	13.3919	30.9643	5.0926	3.6171	0.3600
DenseFuse	34.0135	8.5541	6.6740	1.3491	0.4173	0.3857	13.3480	30.6655	3.9885	3.2740	0.3916
FusionGan	35.4048	8.6400	7.1753	0.8671	0.3410	0.3609	14.3507	42.3040	3.9243	3.3469	0.2591
IFCNN	57.6653	15.0677	6.9730	1.3801	0.4032	0.3456	13.9460	35.8183	7.0401	5.6242	0.5100
MDLatLRR	36.9468	9.3638	6.7171	1.3636	0.4241	0.3875	13.4342	31.3505	4.3216	3.5530	0.4483
NestFuse	53.9286	14.2820	7.3598	1.2597	0.4342	0.3484	14.7196	48.9920	6.2840	5.1834	0.4758
FusionDN	63.1690	16.7138	7.5323	1.1882	0.3621	0.3009	15.0646	55.0559	7.7925	6.4950	0.4631
U2Fusion	66.2529	15.8242	7.1969	1.3551	0.3717	0.3199	14.3938	42.9368	7.5930	6.3133	0.5112
Ours	max + avg	39.4996	10.7670	6.7575	1.3394	0.3151	0.2311	13.5150	31.6977	4.8180	3.8643
	max + max	39.7592	10.6215	6.8186	1.3223	0.3171	0.2217	13.6371	39.6907	4.7275	3.8575
	add + avg	64.5832	16.5082	6.9535	1.4087	0.4295	0.3883	13.9071	35.7447	7.7606	6.2775
	add + max	63.4740	16.1703	6.9666	1.3774	0.4076	0.3640	13.9332	43.2688	7.5247	6.1431

the mutual information (MI, FMI_w and FMI_{dct}) and some complex calculation methods(QG).

We compare the proposed method with ten other excellent methods, and the results of the average values for all fused

images shown in Table II and Table III respectively. The best value in the quality table is made bold in **red and bold**, and the second best value is given in **bold and italic**.

It can be seen from Table II and Table III that our proposed

method obtains eleven best values and four second best values. On the TNO dataset, our method (*add+max*) obtains one best result and six second best results. On the RoadScene dataset, our method (*add + avg*) obtained two best results and four second best results. Comparing with other operator in fusion strategy, the addition operator of high frequency information can achieve better results in several indicators. Although our method does not get the best results in every result, it was able to get second best results in many indicators.

V. CONCLUSIONS

In this paper, we propose a novel multi-network for image decomposition. We also develop a decomposition network fusion framework to fuse infrared images and visible light images. Firstly, with the help of decomposition networks, the infrared image and the visible light image are decomposed into multiple high-frequency feature images and a low-frequency feature image, respectively. Secondly, the corresponding feature image is fused with a specific fusion strategy to obtain the fusion feature images. Finally, the fusion feature images are added pixel by pixel to obtain the fused image. This kind of image decomposition network is universal, and any number of images can be quickly and effectively decomposed by neural network. At the same time, using the power of GPUS, neural networks can easily use GPU for matrix calculation acceleration. The speed of image decomposition can also be very fast. We have performed a subjective and objective evaluation of the proposed method, and the experimental results show that it has reached the state of the art. Although the network structure is simple, it proves the feasibility of the neural network to decompose the image. We have a conjecture that CNN uses the semantics of the image to filter the noise while preserving the edges, and obtain a very good high-frequency information image. We will continue to study image decomposition based on deep learning, including simplifying some originally complex image decomposition calculations such as wavelet transformation, low-rank decomposition, etc., or designing more reasonable network structures for other image processing applications. We think that the network we propose can be used for different image processing tasks, including multi-focus fusion, medical image fusion, multi-exposure fusion, and some basic computer vision tasks such as detection, recognition, and classification. We will then experiment and test this method in other image tasks.

REFERENCES

- [1] J. Ma, Y. Ma, and C. Li, "Infrared and visible image fusion methods and applications: A survey," *Information Fusion*, vol. 45, pp. 153–178, 2019.
- [2] Y. Liu, X. Chen, Z. Wang, Z. J. Wang, R. K. Ward, and X. Wang, "Deep learning for pixel-level image fusion: Recent advances and future prospects," *Information Fusion*, vol. 42, pp. 158–173, 2018.
- [3] T. Mertens, J. Kautz, and F. Van Reeth, "Exposure fusion: A simple and practical alternative to high dynamic range photography," *Computer Graphics Forum*, vol. 28, no. 1, pp. 161–171, 2009.
- [4] Z. Zhang and R. S. Blum, "A categorization of multiscale-decomposition-based image fusion schemes with a performance study for a digital camera application," *Proceedings of the IEEE*, vol. 87, no. 8, pp. 1315–1326, 1999.
- [5] K. P. Upla, M. V. Joshi, and P. P. Gajjar, "An edge preserving multiresolution fusion: Use of contourlet transform and mrf prior," *IEEE Transactions on Geoscience and Remote Sensing*, vol. 53, no. 6, pp. 3210–3220, 2014.
- [6] A. B. Hamza, Y. He, H. Krim, and A. S. Willsky, "A multiscale approach to pixel-level image fusion," *Computer-Aided Engineering*, vol. 12, no. 2, pp. 135–146, 2005.
- [7] J.-j. Zong and T.-s. Qiu, "Medical image fusion based on sparse representation of classified image patches," *Biomedical Signal Processing and Control*, vol. 34, pp. 195–205, 2017.
- [8] Q. Zhang, Y. Fu, H. Li, and J. Zou, "Dictionary learning method for joint sparse representation-based image fusion," *Optical Engineering*, vol. 52, no. 5, p. 057006, 2013.
- [9] Y. Bin, Y. Chao, and H. Guoyu, "Efficient image fusion with approximate sparse representation," *International Journal of Wavelets, Multiresolution and Information Processing*, vol. 14, no. 04, p. 1650024, 2016.
- [10] H. Li and X.-J. Wu, "Multi-focus image fusion using dictionary learning and low-rank representation," in *International Conference on Image and Graphics*. Springer, 2017, pp. 675–686.
- [11] H. Li, X.-J. Wu, and J. Kittler, "Mdlatrr: A novel decomposition method for infrared and visible image fusion," *IEEE Transactions on Image Processing*, 2020.
- [12] Y. Liu, X. Chen, H. Peng, and Z. Wang, "Multi-focus image fusion with a deep convolutional neural network," *Information Fusion*, vol. 36, pp. 191–207, 2017.
- [13] K. R. Prabhakar, V. S. Srikar, and R. V. Babu, "Deepfuse: A deep unsupervised approach for exposure fusion with extreme exposure image pairs," in *ICCV*, 2017, pp. 4724–4732.
- [14] H. Li and X.-J. Wu, "Densefuse: A fusion approach to infrared and visible images," *IEEE Transactions on Image Processing*, vol. 28, no. 5, pp. 2614–2623, 2018.
- [15] Y. Zhang, Y. Liu, P. Sun, H. Yan, X. Zhao, and L. Zhang, "Ifcnn: A general image fusion framework based on convolutional neural network," *Information Fusion*, vol. 54, pp. 99–118, 2020.
- [16] J. Ma, W. Yu, P. Liang, C. Li, and J. Jiang, "Fusiongan: A generative adversarial network for infrared and visible image fusion," *Information Fusion*, vol. 48, pp. 11–26, 2019.
- [17] H. Li, X.-J. Wu, and T. Durrani, "Nestfuse: An infrared and visible image fusion architecture based on nest connection and spatial/channel attention models," *IEEE Transactions on Instrumentation and Measurement*, 2020.
- [18] H. Li, B. S. Manjunath, and S. K. Mitra, "Multisensor image fusion using the wavelet transform," *Graphical Models and Image Processing*, vol. 57, no. 3, pp. 235–245, 1995.
- [19] L. J. Chipman, T. M. Orr, and L. N. Graham, "Wavelets and image fusion," vol. 3, p. 3248, 1995.
- [20] G. Liu and S. Yan, "Latent low-rank representation for subspace segmentation and feature extraction," pp. 1615–1622, 2011.
- [21] A. L. Maas, A. Y. Hannun, and A. Y. Ng, "Rectifier nonlinearities improve neural network acoustic models," in *Proc. icml*, vol. 30, no. 1, 2013, p. 3.
- [22] X. Mao, Q. Li, H. Xie, R. Y. K. Lau, Z. Wang, and S. P. Smolley, "Least squares generative adversarial networks," pp. 2813–2821, 2017.
- [23] T.-Y. Lin, M. Maire, S. Belongie, J. Hays, P. Perona, D. Ramanan, P. Dollár, and C. L. Zitnick, "Microsoft coco: Common objects in context," in *European conference on computer vision*. Springer, 2014, pp. 740–755.
- [24] J. Deng, W. Dong, R. Socher, L.-J. Li, K. Li, and L. Fei-Fei, "Imagenet: A large-scale hierarchical image database," in *2009 IEEE conference on computer vision and pattern recognition*. Ieee, 2009, pp. 248–255.
- [25] A. Toet *et al.*, "Tno image fusion dataset," *Figshare. data*, 2014.
- [26] H. Xu, J. Ma, Z. Le, J. Jiang, and X. Guo, "Fusiondn: A unified densely connected network for image fusion," in *AAAI*, 2020, pp. 12 484–12 491.
- [27] D. P. Kingma and J. Ba, "Adam: A method for stochastic optimization," *arXiv: Learning*, 2014.
- [28] M. D. Zeiler, "Adadelta: An adaptive learning rate method," *arXiv: Learning*, 2012.
- [29] F. Nencini, A. Garzelli, S. Baronti, and L. Alparone, "Remote sensing image fusion using the curvelet transform," *Information fusion*, vol. 8, no. 2, pp. 143–156, 2007.
- [30] J. J. Lewis, R. J. Callaghan, S. G. Nikolov, D. R. Bull, and N. Canagarajah, "Pixel-and-region-based image fusion with complex wavelets," *Information fusion*, vol. 8, no. 2, pp. 119–130, 2007.
- [31] V. Naidu, "Image fusion technique using multi-resolution singular value decomposition," *Defence Science Journal*, vol. 61, no. 5, p. 479, 2011.

- [32] H. Xu, J. Ma, J. Jiang, X. Guo, and H. Ling, "U2fusion: A unified unsupervised image fusion network," *IEEE Transactions on Pattern Analysis and Machine Intelligence*, 2020.
- [33] C. S. Xydeas and V. S. Petrovic, "Objective pixel-level image fusion performance measure," in *Sensor Fusion: Architectures, Algorithms, and Applications IV*, vol. 4051. International Society for Optics and Photonics, 2000, pp. 89–98.
- [34] A. M. Eskicioglu and P. S. Fisher, "Image quality measures and their performance," *IEEE Transactions on communications*, vol. 43, no. 12, pp. 2959–2965, 1995.
- [35] J. W. Roberts, J. A. van Aardt, and F. B. Ahmed, "Assessment of image fusion procedures using entropy, image quality, and multispectral classification," *Journal of Applied Remote Sensing*, vol. 2, no. 1, p. 023522, 2008.
- [36] V. Aslantas and E. Bendes, "A new image quality metric for image fusion: the sum of the correlations of differences," *Aeu-international Journal of electronics and communications*, vol. 69, no. 12, pp. 1890–1896, 2015.
- [37] M. Haghigat and M. A. Razian, "Fast-fmi: non-reference image fusion metric," in *2014 IEEE 8th International Conference on Application of Information and Communication Technologies (AICT)*. IEEE, 2014, pp. 1–3.
- [38] H. Peng, F. Long, and C. Ding, "Feature selection based on mutual information criteria of max-dependency, max-relevance, and min-redundancy," *IEEE Transactions on Pattern Analysis and Machine Intelligence*, vol. 27, no. 8, pp. 1226–1238, 2005.
- [39] X. Desheng, "Research of measurement for digital image definition," *Journal of Image and Graphics*, 2004.
- [40] G. Cui, H. Feng, Z. Xu, Q. Li, and Y. Chen, "Detail preserved fusion of visible and infrared images using regional saliency extraction and multi-scale image decomposition," *Optics Communications*, vol. 341, pp. 199–209, 2015.



Josef Kittler (Life Member, IEEE) received the B.A., Ph.D., and D.Sc. degrees from the University of Cambridge, in 1971, 1974, and 1991, respectively.

He is currently a Distinguished Professor of machine intelligence at Centre for Vision, Speech and Signal Processing, University of Surrey, Guildford, U.K. He conducts research on biometrics, video and image database retrieval, medical image analysis, and cognitive vision. He published the textbook *Pattern Recognition: A Statistical Approach* and over 700 scientific papers. His publications have been cited over 60,000 times (Google Scholar). He is a Series Editor of *Lecture Notes in Computer Science* (Springer). He currently serves on the Editorial Boards of *Pattern Recognition Letters*, *International Journal of Pattern Recognition and Artificial Intelligence*, and *Pattern Analysis and Applications*. He has also served as a member of the Editorial Board for the *IEEE TRANSACTIONS ON PATTERN ANALYSIS AND MACHINE INTELLIGENCE* from 1982 to 1985. He served on the Governing Board of the International Association for Pattern Recognition (IAPR), as one of the two British representatives, from 1982 to 2005, and the President of the IAPR from 1994 to 1996.



Yu Fu received the B.M. degree in professional engineering management from North China Institute Of Science And Technology, China. He is currently a Master student in the Jiangsu Provincial Engineering Laboratory of Pattern Recognition and Computational Intelligence, Jiangnan University. His research interests include image fusion, machine learning and deep learning.



Xiao-Jun Wu received the B.Sc. degree in mathematics from Nanjing Normal University, Nanjing, China, in 1991, and the M.S. and Ph.D. degrees in pattern recognition and intelligent system from the Nanjing University of Science and Technology, Nanjing, in 1996 and 2002, respectively.

From 1996 to 2006, he taught at the School of Electronics and Information, Jiangsu University of Science and Technology, where he was promoted to a Professor. He was a Fellow of the International Institute for Software Technology, United Nations University, from 1999 to 2000. He was a Visiting Researcher with the Centre for Vision, Speech, and Signal Processing (CVSSP), University of Surrey, U.K., from 2003 to 2004. Since 2006, he has been with the School of Information Engineering, Jiangnan University, where he is currently a Professor of pattern recognition and computational intelligence. His current research interests include pattern recognition, computer vision, and computational intelligence. He has published over 300 articles in his fields of research. He was a recipient of the Most Outstanding Postgraduate Award from the Nanjing University of Science and Technology.